

Enhanced Carrier Transport along Edges of Graphene

Devices

Jungseok Chae^{†§}, Suyong Jung^{‡§}, Sungjong Woo^{||}, Hongwoo Baek[†], Jeonghoon Ha[†], Young Jae Song^{‡§},

Young-Woo Son^{||}, Nikolai B. Zhitenev[‡], Joseph A. Stroscio[‡], and Young Kuk^{†*}

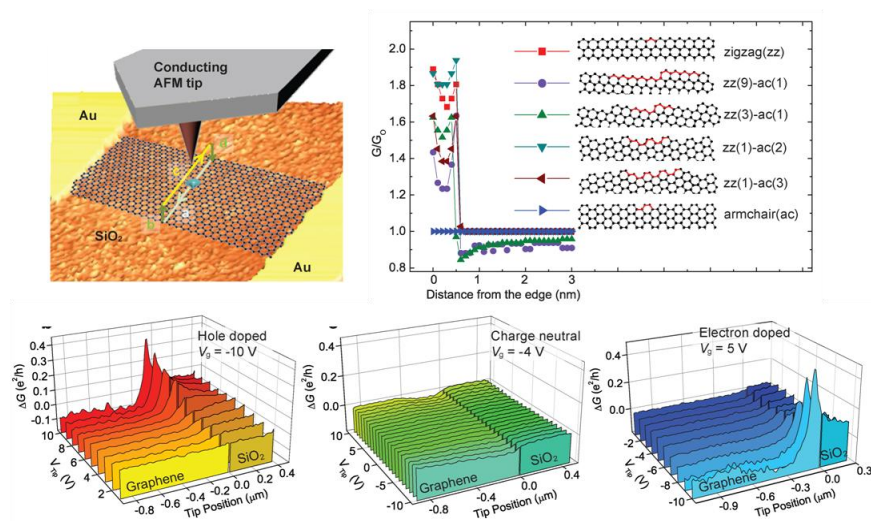
[†]Department of Physics and Astronomy, Seoul National University, Seoul 151-747, Korea

[‡]Center for Nanoscale Science and Technology, NIST, Gaithersburg, MD 20899, USA

[§]Maryland NanoCenter, University of Maryland, College Park, MD 20742, USA

^{||}Korea Institute for Advanced Study, Seoul 130-722, Korea

Table of Contents Graphic



ABSTRACT

The relation between macroscopic charge transport properties and microscopic carrier distribution is one of the central issues in the physics and future applications of graphene devices (GDs). We find strong conductance enhancement at the edges of GDs using scanning gate microscopy. This result is explained by our theoretical model of the opening of an additional conduction channel localized at the edges by depleting accumulated charge by the tip.

KEYWORDS : Graphene, Edge, Edge state, Scanning gate microscopy

MANUSCRIPT TEXT

Electronic states located at a surface with energies near the Fermi level lying within the bulk band gap can significantly contribute to a material's overall conductance, for example, as in the case of topological insulators. Similarly, when extra edge states are present at cut edges of a graphene stripe near the Dirac point^{1,2}, they may completely alter the existing transport models mostly considering carrier scattering in the bulk stripe. A substantial portion of the transport current may flow through the edge states without much carrier scattering. The unique properties of edge states have been addressed in many theoretical studies. Moreover, unique graphene devices (GDs) that have no analog in conventional semiconductor electronics have been proposed, such as a pseudo-spin filter³, which depend on the graphene edge termination. For narrower graphene strips such as in nano-ribbon devices, the contribution of the edge states become even more substantial^{4,5}. Central to all these issues is the question, "How does the geometric and electronic structure of a graphene edge affect the carrier transport?" This problem is barely addressed experimentally through conventional transport measurements because it is extremely difficult to isolate the transport current through the edges from the bulk in conventional current-voltage (I-V) measurements.

Here, we have used a scanning gate microscope (SGM) with x-y positioning motors as an experimental tool to probe the impact of the edge effects on the transport properties of GDs. In SGM, a conductive atomic force microscope (AFM) tip was used as a local top gate to induce an electrostatic potential and alter the Fermi level and the carrier density over the selected area of interest⁶⁻⁸. The transport signal change (conductance variation (ΔG)) in the presence of the AFM tip-gate revealed how the local electronic structure of a sample contributes to its macroscopic transport properties. The utility of SGM has been demonstrated in other two-dimensional electron gas (2DEG) systems by probing carrier scattering from impurities⁹, single electron charging effects¹⁰, quantum confinement, and coherent electron flows¹¹⁻¹³. The exposure of the graphene surface and the presence of a back gate have facilitated SGM microscopic studies at a density range and with spatial resolution far exceeding those in previous SGM studies of semiconductor 2DEG. The required accuracy of tip positioning was achieved using a precise sample stage and a high resolution optical microscope equipped for the SGM setup (Fig. S1 and Movie S1). All the data presented in this letter is obtained in liquid nitrogen temperature.

In this study, we present SGM measurements of a single-layer GD fabricated on a Si/SiO₂ substrate¹⁴. We observe an unexpected conductance enhancement along the edges of charged GDs dependent on the sign of charge carriers and the polarity of the tip-gating bias. Inside the GDs, the effect of gating by the AFM tip is qualitatively similar to a back-gate electrode. We attribute conductance enhancements at the edge of doped GDs to the opening of an additional conduction channel induced by the charge accumulation and the corresponding shift of the local Dirac point at the graphene edges (Fig. 1a) and local tip-gating. Our experimental observations are successfully explained by an electrostatic model and electronic structure calculations.

AFM topographic images were obtained by employing a non-invasive, non-contact frequency modulation mode^{15,16}. Figure 1b is a topographic image of a GD that shows a clear distinction between the underlying SiO₂, the graphene layer, and the edges of the graphene flake. The magnified image reveals graphene topographic corrugation expected for exfoliated flakes (inset of Fig. 1b). To ensure non-invasive SGM measurements at a corrugated graphene surface, the AFM and SGM are performed in

sequential scans as illustrated in Fig. 1c. After the first AFM line scan ((a) in Fig. 1c), the tip is lifted by a pre-defined height, ≈ 10 nm ((b) in Fig. 1c). Then, in the SGM line scan ((c) in Fig. 1c), the tip follows the topography profile recorded in the previous AFM scan with a voltage applied to the tip, while monitoring dc conductance ($G=I/V$) variation across the two-probe source-drain metal contacts. The back-gate is used to tune the Fermi energy (E_F) with respect to the Dirac point, controlling the carrier type, electron or hole, and the carrier density inside the GDs. After finishing the SGM line scan, the tip is re-approached to the surface ((d) in Fig. 1c) without a tip-gating bias to prepare for the next AFM line scan.

Figure 1d shows how local tip-gating affects the dc conductance of a GD. For this measurement, the AFM tip is positioned at the center of a GD and the back-gate voltage is set at the charge neutrality point ($V_D = -6$ V). In a similar way to the back-gating results, the conductance increases with tip-gate voltage. With an applied electric field from a biased AFM tip, additional charged carriers are induced locally in the graphene channel, resulting in increased conductance. Inside the bulk channel of a GD, the AFM tip is acting like a typical top-gate electrode¹⁷.

We now focus on how the SGM signal changes at the edge of the GDs in the presence of a local tip-gating electrode. As shown in a topographic image of the GD in Fig. 2a, the edge of the GD is located at the top-left corner. In this device, the charge neutrality point is measured at $V_g = -15$ V. When $V_{\text{Tip}} = 0$ V (Fig. 2b), the SGM signal is similar throughout the GD. However, the difference between the edge and the interior of the graphene becomes dramatic when a negative V_{Tip} is applied (Fig. 2c). As shown in Fig. 2c, the SGM signal at the edge is enhanced by a factor of 10 compared with those inside the GD. Interestingly, there is no such SGM signal enhancement when a positive V_{Tip} is applied (Fig. 2d). The dependence of the SGM signal on V_{Tip} measured with the tip positioned at the edge shown in Fig. 2e is very different from the bulk response. When the back-gate is set at $V_D + 15$ V, i.e. $V_g = 0$ V, the conductance should decrease with decreasing tip-gate voltage, indicated by the solid black line in Fig. 2e. When the tip is located at the edge, however, the conductance increases at negative V_{Tip} . This suggests that the conductance enhancement at the edge is related to the presence of the graphene edge

and its electronic structure, not to the electrostatically induced charges between the tip and the GDs as observed inside the bulk channel.

To further investigate the origin of the conductance enhancement at the edges, we performed the same SGM measurements with varying carrier density and sign in another GD with a charge neutrality point of $V_g = -4$ V. The width and length of graphene channel are $1.6 \mu\text{m}$ and $2.3 \mu\text{m}$, respectively. Figure 3a shows the macroscopic conductance as a function of back-gate voltage. Figures 3b-d show V_{Tip} -dependent SGM line profiles measured across the edge with the carrier density corresponding to hole-doped (Fig. 3b), charge neutrality point (Fig. 3c) and electron-doped (Fig. 3d). For these measurements, the SGM signal is recorded at a fixed back-gate voltage and at different tip-gate voltages between -10 V and 10 V.

At the charge neutrality point, $V_g = -4$ V (Fig. 3c), the SGM signal is similar at the edge and in the interior of the GD within the range of V_{Tip} from -10 V to 10 V. However, when the GD is hole-doped at $V_g = -10$ V (Fig. 3b), a conductance enhancement at the edge is observed, only at positive V_{Tip} . Conversely, the same conductance enhancement at the edge is seen at negative V_{Tip} for the electron-doped GD at $V_g = 5$ V (Fig. 3d). These observations are consistent with those in Fig. 2.

The spatial variation of the SGM signals shown in Figs. 3e-g reveals that conductance enhancement is nearly constant along the edge. Each SGM map in Figs. 3e-g ($1.3 \mu\text{m} \times 1.3 \mu\text{m}$) is obtained at the same gate voltages as Figs. 3b-d; hole-doped ($V_g = -10$ V for Figs. 3b and e), charge neutral ($V_g = -4$ V for Figs. 3c and f), and electron-doped ($V_g = 10$ V for Figs. 3d and g), and with the tip-gating voltage set at $V_{\text{Tip}} = 10$ V for both Figs. 3e and f and at $V_{\text{Tip}} = -10$ V for Fig. 3g. The conductance enhancement at the edge is measured up to $0.3 G_0$ ($= e^2/h$) and shows little dependence on spatial location along the graphene edge.

Several scenarios can be considered for the origin of the observed SGM results of the graphene edge. First, a suppression of scattering by randomly distributed impurities or local disorder along the edges may result in the conductance enhancement. However, that can be ruled out because the charge-transport mechanism in our GDs is diffusive and the observed conductance enhancement is homogeneous along

the edges over a micrometer scale. Second, the variations in inter-edge scattering in the presence of a SGM tip potential can be also ruled out because the width of our GDs is wider than one micrometer.

Third, from the experimental result that the conductance enhancement at the edge is not observed in a neutral GD but only in a doped GD, we can infer that the charge accumulation at the true 2D edges of a graphene strip may result in the conductance enhancement. In a doped GD, the excess charge shows strong accumulation diverging as $x^{-1/2}$ at the edge¹⁸ by the diverging electrostatic potential at edge as shown in the electrostatic calculation (Fig. S3). From the linear dispersion relation of graphene near the \mathbf{K} point, the local variation of the Dirac point, E_D , referenced to the constant Fermi level, E_F , as a function of excess electron density, can be approximately deduced as $E_D(n_e)/E_F = -\text{sgn}(n_e) (|n_e|/n_o)^{1/2}$, where $n_o = 8.225 \times 10^{13} \text{ cm}^{-2}$, as illustrated in Fig. 1a. However, this effect alone cannot explain the observed tip bias dependence. We measured the conductance enhancement at the edges of the GD by applying a tip bias which depletes the existing charge. For example, in an electron-doped GD, the conductance should decrease while decreasing the negative tip bias but the measured data increases with decreasing negative tip bias as shown in Fig. 2e.

Fourth, one can consider a model in which localized states at the edge^{1,19} and the charge accumulation are incorporated together. The localized edge states with a flat dispersion have been recently observed in scanning tunneling spectroscopy measurements¹⁹. In this model, the enhancement mechanism may arise from the opening of an edge conductance channel by the tip gating potential. In order to demonstrate that this model explains the observed results, the electronic structure and the transport properties are calculated using a tight-binding Hamiltonian and quantum scattering theory² with modulation of the on-site energy of each carbon atom to incorporate the shift of the Dirac point across the device.

The calculation for GNRs with homogeneous zigzag-shaped edges shows that the overall band structure is shifted by $E_D(n_e)$ since the region with strong charge accumulation is relatively narrow, and there the shift of the Dirac point at the edge is $E_D(n_{e,\text{GNR}}(x = w_G/2))$. However, there is a significant new outcome; the states which were originally in a flat band of zigzag-shaped edges (Fig. 4a) now curve downward due to the accumulated charge density at the edge (Fig. 4b). Such dispersion change creates two

additional degenerate channels curving down as shown in Fig. 4b, or the *edge* band. The channels are, however, below the Fermi level so that no additional conductance is gained at the Fermi level in the GD. To understand the origin of increased conductance, we calculated local Dirac point variations across a GD, based on electrostatic analysis and the tip gating effect. The calculation of Dirac point variations from the Fermi level, $E_D(n_{e,\text{tot}}(x)) - E_F$, along the lateral distance at the central axis of the GD, shows a charge inversion under the tip position with sufficient tip-gating voltage, where $n_{e,\text{tot}}(x)$ is the total excess electron density by the tip and the GNR. For $V_g = 10$ V (electron-doped, corresponding to the experimental parameter in Fig. 3d) and tip height of 30 nm, we can obtain a protrusion of $n_{e,\text{tot}}(x)$ near the tip position with $V_{\text{Tip}} = -3$ V. However, with $V_{\text{Tip}} = -5$ V, the electric field is strong enough to induce the charge inversion and a local hole domain under the tip. As the tip moves toward the edge, the symmetry of the two GD edges is broken so that the degeneracy of the edge band is lifted. When the tip is positioned at the edge, the band structure at the Brillouin zone boundary of the corresponding localized edge state is bent upward and crosses the Fermi level as shown in Fig. 4c. The crossover is related to the local inversion, from electron to hole-doping at the graphene edge due to the tip potential. This crossing at the Fermi level provides an additional conduction channel and shows the basic physics of the conductance enhancement at the edge of the GD.

To illustrate the mechanism for the conductance enhancement, we calculate the conductance through the GD based on the Landauer formula including the thermal broadening of the Fermi-Dirac distribution. This calculation is meant to illustrate the mechanism and the order of magnitude of the enhancement. Figure 4d shows the simulated conductance enhancement for different atomic edge structures. The conductance enhancement caused by the additional channel formed at the edge is insensitive to the detailed atomic configurations along the edges. We note that the conductance enhancement is predicted with small portions of ‘zigzag’ structure at the edge with the single exception: the perfect armchair-edged GNR shows no conductance enhancement because the flat band at the Fermi level (shown in Fig. 4a for ‘zigzag’ structure) does not exist for a perfect armchair-edged GNR, which cause electrons to delocalize away from the edges so that the localized electric field from the conducting tip does not affect

transport as much. The robustness of the enhancement and the homogeneous response along the edge is dictated by the crossover of the *single channel*; the cross-over occurs exactly “once” independent of the width of the flat band. We have observed this conductance enhancement in all measured GDs, suggesting that there are different atomic structures at the edges including the zigzag structure. In this model, a two-dimensional extension of a one-dimensional model is used to find the physical origin that produces the conductance enhancement. Further study is needed to obtain quantitative agreement with the experimental data.

The magnitude of the observed conductance enhancement can be used to estimate the approximate lateral extent of the tip gating field. The lateral extent is strongly dependent on the tip potential. The extent is certainly larger than the apparent peak width of the SGM signal at the edge. As the tip is moved away from the edge into the bulk, the signal drop is affected by the shrinking of the inverted channel along the edge. From Fig. 3, the maximum conductance enhancement is $\approx 0.3 G_0$, which is about an 8 % change in total conductance. For the estimate, we assume that the conductance is mainly determined by the two device edges and that the inverted channel is perfectly conducting yielding the extent of the channel to be ≈ 370 nm, or 16 % (the factor of 2 arises since other edge is unaffected) of the device length, at the highest tip potentials of ± 10 V. The same estimate at lower tip potential yields the lateral extent of the gating to be ≈ 100 nm at $V_{\text{Tip}} = -2$ V. This is consistent with another estimate based on the maximal amplitude of the SGM signal in the bulk (Fig. S2) indicating an effective length scale of ≈ 100 nm at a tip potential of 2.5V. Therefore, the effective length scale by the tip can be extended to 400~500 nm at the tip voltage of ± 10 V and it is compatible to the estimated length scale in the experimental data. Therefore as the gating tip moves 250~250 nm away from graphene edges at ± 10 V, the SGN signal should decrease to the bulk value as shown in Figs. 3(b) and (d).

In conclusion, our SGM measurements demonstrate that the edge of a graphene sheet contributes to the transport properties very differently compared to an edge in a more conventional semiconductor 2DEG. The difference is caused by the band structure of graphene and by the atomic sharpness of the edge. The edge transport is significant even in a wide GD at high charge density, which is typical for many

potential applications. In narrow devices, such as a GNR, the edge transport becomes even more important for the proper understanding of its transport properties and the design of devices.

Acknowledgement

This work was supported in part by the Korea Research Foundation Grant (MOEHRD) (KRF-2006-0093847, KRF-2010-00349). Y.-W. S. was supported in part by the NRF grant funded by the government of Korea, MEST (QMMRC, R11-2008-053-01002-0). We acknowledge computational support from the CAC of KIAS

Supporting Information Available.

REFERENCES and NOTES

- (1) Nakada, K. Fujita, M. Dresselhaus, G.; Dresselhaus, M. S. *Phys. Rev. B* **1996**, *54*, 17954.
- (2) Son, Y.-W. Cohen, M. L.; Louie, S. G. *Nature* **2006**, *444*, 347-349.
- (3) Rycerz, A. Tworzydło, J.; Beenakker, C. W. J. *Nat Phys* **2007**, *3*, 172-175.
- (4) Son, Y.-W. Cohen, M. L.; Louie, S. G. *Phys. Rev. Lett.* **2006**, *97*, 216803.
- (5) Han, M. Y. Özyilmaz, B. Zhang, Y.; Kim, P. *Phys. Rev. Lett.* **2007**, *98*, 206805.
- (6) Heller, E. J. Aidala, K. E. LeRoy, B. J. Bleszynski, A. C. Kalben, A. Westervelt, R. M. Maranowski, K. D.; Gossard, A. C. *Nano Letters* **2005**, *5*, 1285-1292.
- (7) Freyn, A. Kleftogiannis, I.; Pichard, J.-L. *Phys. Rev. Lett.* **2008**, *100*, 226802.
- (8) Pala, M. G. Hackens, B. Martins, F. Sellier, H. Bayot, V. Huant, S.; Ouisse, T. *Phys. Rev. B* **2008**, *77*, 125310.
- (9) Hsu, J. W. P. Weimann, N. G. Manfra, M. J. West, K. W. Lang, D. V. Schrey, F. F. Mitrofanov, O.; Molnar, R. J. *Appl. Phys. Lett.* **2003**, *83*, 4559.
- (10) Hackens, B. Martins, F. Ouisse, T. Sellier, H. Bollaert, S. Wallart, X. Cappy, A. Chevrier, J. Bayot, V.; Huant, S. *Nat Phys* **2006**, *2*, 826-830.
- (11) Topinka, M. A. LeRoy, B. J. Westervelt, R. M. Shaw, S. E. J. Fleischmann, R. Heller, E. J. Maranowski, K. D.; Gossard, A. C. *Nature* **2001**, *410*, 183-186.
- (12) Aidala, K. E. Parrott, R. E. Kramer, T. Heller, E. J. Westervelt, R. M. Hanson, M. P.; Gossard, A. C. *Nat Phys* **2007**, *3*, 464-468.
- (13) Jura, M. P. Topinka, M. A. Urban, L. Yazdani, A. Shtrikman, H. Pfeiffer, L. N. West, K. W.; Goldhaber-Gordon, D. *Nat Phys* **2007**, *3*, 841-845.
- (14) Novoselov, K. S. Jiang, D. Schedin, F. Booth, T. J. Khotkevich, V. V. Morozov, S. V.; Geim, A. K. *Proceedings of the National Academy of Sciences of the United States of America* **2005**, *102*, 10451-10453.
- (15) Albrecht, T. R. Grütter, P. Horne, D.; Rugar, D. *J. Appl. Phys.* **1991**, *69*, 668.

- (16) Giessibl, F. J.; Bielefeldt, H. *Phys. Rev. B* **2000**, *61*, 9968.
- (17) Williams, J. R. DiCarlo, L.; Marcus, C. M. *Science* **2007**, *317*, 638-641.
- (18) Silvestrov, P. G.; Efetov, K. B. *Phys. Rev. B* **2008**, *77*, 155436.
- (19) Tao, C. Jiao, L. Yazyev, O. V. Chen, Y.-C. Feng, J. Zhang, X. Capaz, R. B. Tour, J. M. Zettl, A. Louie, S. G. Dai, H.; Crommie, M. F. *Nat Phys* **2011**, *7*, 616-620.

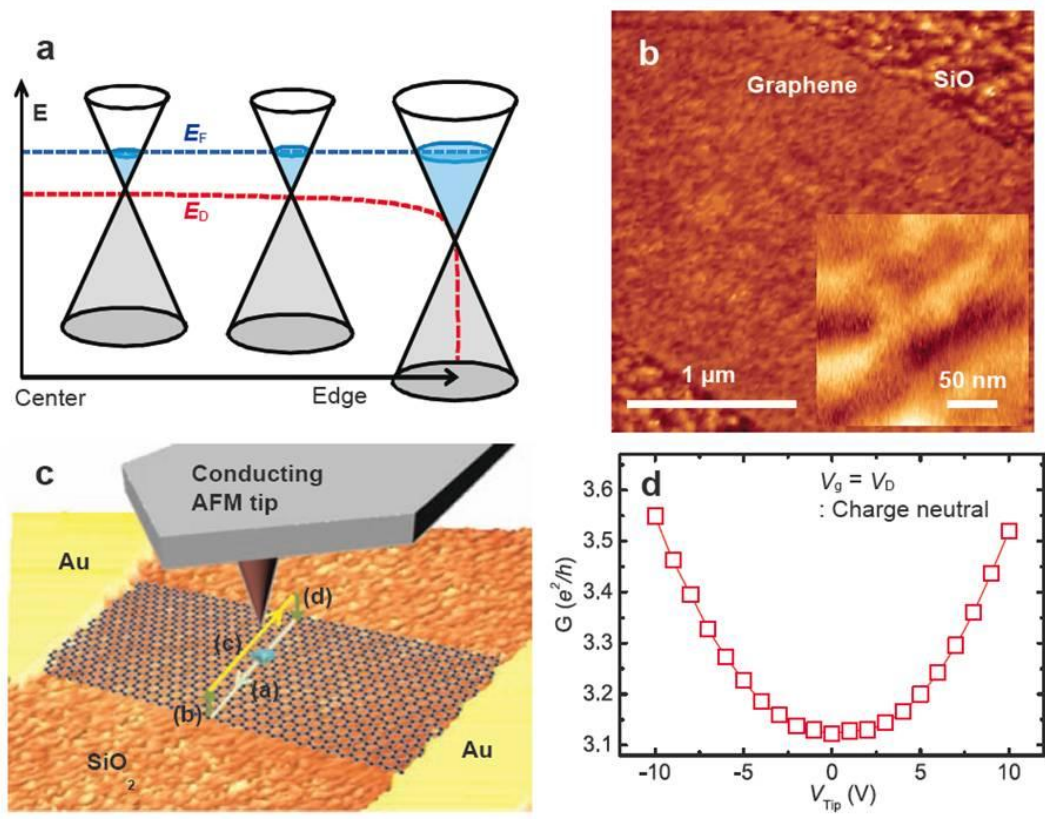


Figure 1. Graphene device and SGM measurement. (a) Schematic view of Dirac point (E_D) variation from the center to the edge of electron-doped graphene device. The local Dirac point is bent near the edge of doped-graphene due to the accumulated charge at the edge. (b) AFM topography image of the graphene device. The step edge between graphene and SiO₂ are located at both top-right and bottom-left corners. Inset: Magnified image of graphene area showing corrugation from the SiO₂ substrate. (c) Schematic diagram of SGM measurements. The basic principle of SGM operations from (a) to (d) are explained in the main text. The blue dot under the conductive AFM tip indicates the area strongly affected by the electrostatic field from the tip. (d) Conductance as a function of tip-gating voltages measured across two Au-contact electrodes (Fig. 1c). The back-gate voltage is set at the charge neutrality point (V_D) and the tip position is fixed at the center of graphene device.

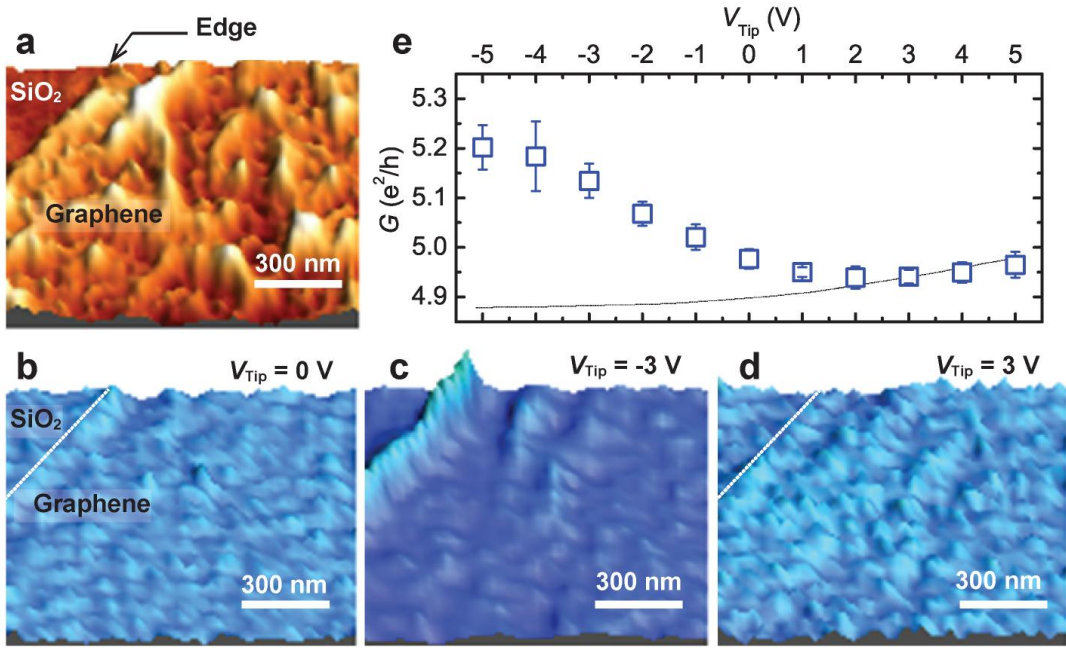


Figure 2. Conductance enhancement at the edge of a graphene device. (a) AFM topography image of graphene device showing corrugation in the graphene area and the step edge with SiO₂ located at top-left corner. (b-d) SGM maps obtained at the same location as Fig. 2a with different tip-gating voltages of $V_{\text{Tip}} = 0 \text{ V}$ (b), $V_{\text{Tip}} = -3 \text{ V}$ (c), and $V_{\text{Tip}} = 3 \text{ V}$ (d). The back-gate voltage is set at $V_g = 0 \text{ V}$, at which graphene is doped with electrons at a density of $1.22 \times 10^{12} \text{ cm}^{-2}$. Conductance change is represented by color scale from purple (low) to light-blue (high): the plot range of each SGM map is (b) (4.93 to 4.96) G_0 , (c) (4.95 to 5.23) G_0 , and (d) (4.95 to 4.98) G_0 . Conductance enhancement at the edge of graphene device with negative tip-gating voltage is clearly shown in Fig. 2c. (e) Conductance as a function of tip-gating voltage at the edge of graphene-SiO₂ interface. The data is averaged over the values along the edge and uncertainties represent one standard deviation. The back-gate voltage is set at $V_g = 0 \text{ V}$, which is shifted away by 15 V from the charge neutrality point (electron doped). A solid black line shows an expected conductance behavior with the tip positioned at the center of the GD.

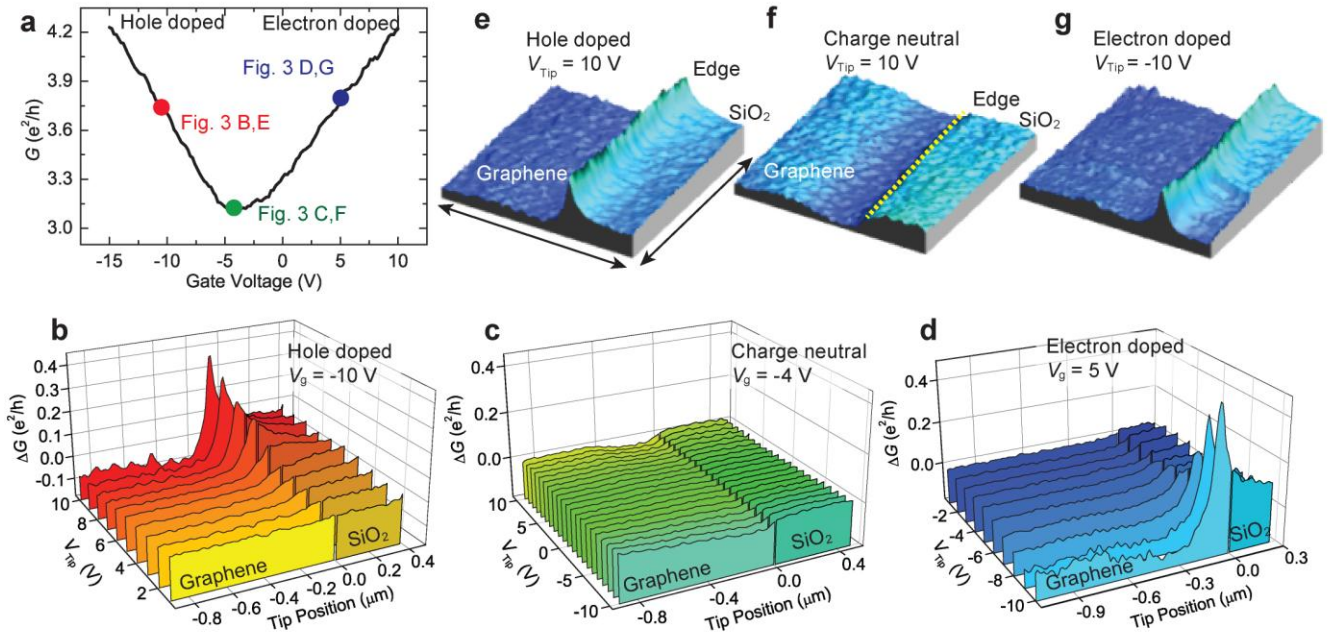


Figure 3. Carrier density-dependent conductance enhancement at the edge of a graphene device. (a) Conductance as a function of back-gate voltage without tip-gating. The charge neutrality point of the device is measured around $V_g = -4$ V. The width and length of the graphene channel are $1.6 \mu\text{m}$ and $2.3 \mu\text{m}$, respectively. The red, green and blue dots indicate back-gate voltages for each SGM measurement in Figs. 3b and e ($V_g = -10$ V, hole doped), 3c and f ($V_g = -4$ V, charge neutral), and 3d and g ($V_g = 5$ V, electron doped), respectively. (b-d) SGM measurements as a function of tip-gating voltage across the edge of the graphene device. The back-gate voltage is adjusted to modulate the doping-level inside the device from hole-doped ($V_g = -10$ V, Fig. 3b), charge neutral ($V_g = -4$ V, Fig. 3c), and electron-doped ($V_g = 5$ V, Fig. 3d). Two-probe conductance at a fixed tip-gating voltage is recorded while the conducting tip scans across the edge. The conductance shift (ΔG) is obtained from the value at the farthest position of SiO_2 from the edge and is plotted at different tip locations. (e-g) SGM maps across the edge of the graphene device. Scanning parameters: (e) $V_g = -10$ V, $V_{\text{Tip}} = 10$ V, (f) $V_g = -4$ V, $V_{\text{Tip}} = 10$ V and (g) $V_g = 5$ V, $V_{\text{Tip}} = -10$ V. The location of the graphene flake, the SiO_2 and their boundary are indicated in Figs. 3e and 3f. The black arrows in Fig. 3e represent the length scale of $1.3 \mu\text{m}$. The same color scale as Figs. 2b-d is used. The range of conductance shift for each map is (e) $0.53 G_0$, (f) $0.05 G_0$, and (g) $0.69 G_0$.

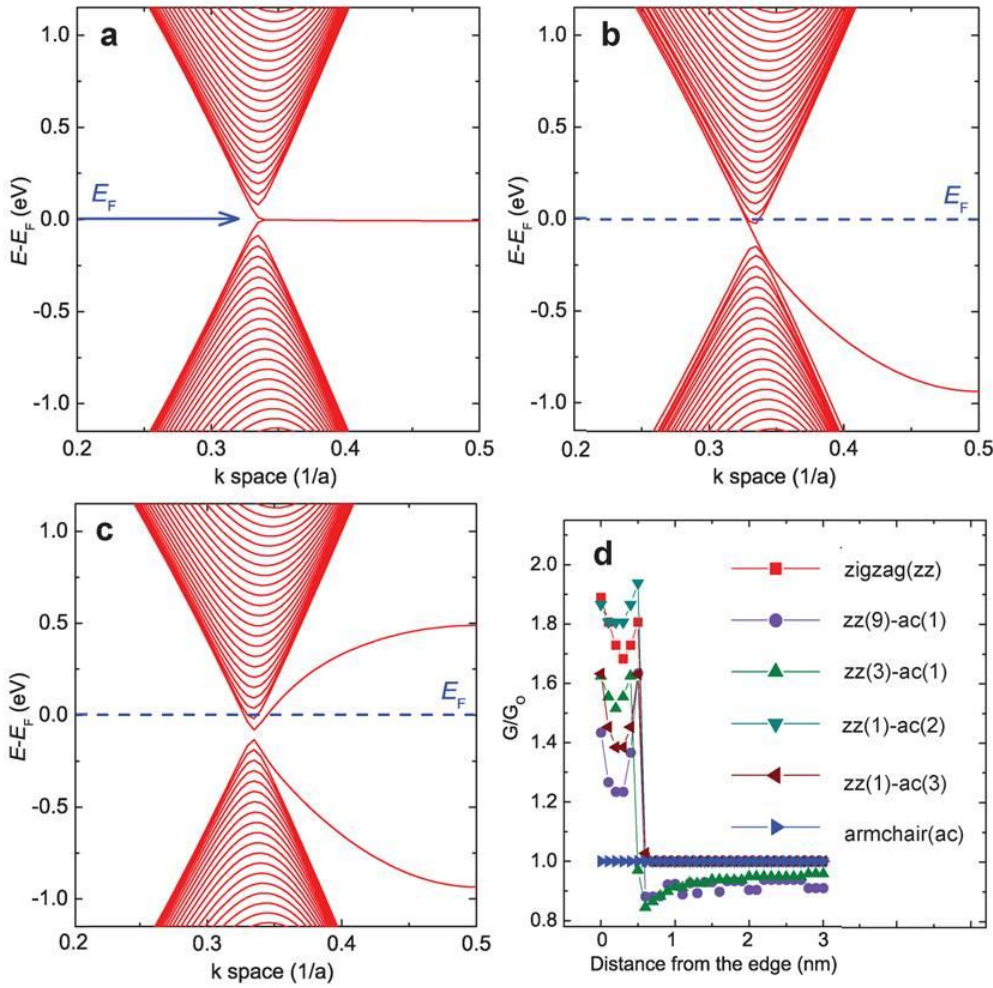


Figure 4. Theoretical model for the conductance enhancement at the edge of a graphene device. (a-c) Band diagrams of a zigzag-edged graphene device with half-width of 17 nm in the cases of charge-neutral (a), electron-doped (b), and electron-doped with a biased-tip positioned at the edge (c). In Fig. 4b, the flat band existed at the Fermi-level (Fig. 4a) is bent toward the valence band since the energies of localized states at the graphene device edge follow the Dirac point shift. In Fig. 4c, the degeneracy of the curved flat band is lifted due to the electric field from the conducting tip and eventually one of them crosses the Fermi-level resulting in an additional conduction channel at the Fermi-level. (d) Conductance variation as a function of tip location from the edge to the center of the device at various graphene edge configurations. A Gaussian tip width of 0.75 nm is used for the calculation. The ratio between the number of zigzag (zz) and armchair (ac) chains does not affect the conductance enhancement.

SUPPORTING INFORMATION PARAGRAPH

1 Supplementary Methods

1.1 Device Characteristics and Characteristics

1.2 in-situ Alignment and SGM Measurement

2 Supplementary Data

2.1 Effective Range of Tip-gating

2.2 SGM Modeling for Theoretical Calculations

3 Supplementary Notes

3.1 References

4 Supplementary Figures

Supplementary Video, file name: “Movie S1. operation of in-situ motors.wmv”